Plasmon-enhanced polymer photovoltaic cells based on large aspect ratio gold nanorods and the related working mechanism

Chen, S. F.; Cheng, F.; Mei, Y.; Peng, B.; Kong, M.; Hao, J. Y.; Zhang, R.; Xiong, Q. H.; Wang, L. H.; Huang, W.

2014

Chen, S. F., Cheng, F., Mei, Y., Peng, B., Kong, M., Hao, J. Y., et al. (2014). Plasmon-enhanced polymer photovoltaic cells based on large aspect ratio gold nanorods and the related working mechanism. Applied Physics Letters, 104(21), 213903-.

https://hdl.handle.net/10356/103708

https://doi.org/10.1063/1.4880575

Plasmon-enhanced polymer photovoltaic cells based on large aspect ratio gold nanorods and the related working mechanism

S. F. Chen, F. Cheng, Y. Mei, B. Peng, M. Kong, J. Y. Hao, R. Zhang, Q. H. Xiong, L. H. Wang, and W. Huang

Citation: Applied Physics Letters **104**, 213903 (2014); doi: 10.1063/1.4880575
View online: http://dx.doi.org/10.1063/1.4880575
View Table of Contents: http://scitation.aip.org/content/aip/journal/apl/104/21?ver=pdfcov
Published by the AIP Publishing

Plasmon-enhanced polymer photovoltaic cells based on large aspect ratio gold nanorods and the related working mechanism

S. F. Chen,[1] F. Cheng,[1,a)] Y. Mei,[1,a)] B. Peng,[2,a)] M. Kong,[1] J. Y. Hao,[1] R. Zhang,[1] Q. H. Xiong,[2,3,b)] L. H. Wang,[1] and W. Huang[1,4,b)]
[1]*Key Laboratory for Organic Electronics and Information Displays (KLOEID) and Institute of Advanced Materials (IAM), Nanjing University of Posts and Telecommunications, Nanjing 210023, China*
[2]*Division of Physics and Applied Physics, School of Physical and Mathematical Sciences, Nanyang Technological University, Singapore 637371*
[3]*NOVITAS, Nanoelectronics Centre of Excellence, School of Electrical and Electronic Engineering, Nanyang Technological University, Singapore 639798*
[4]*Jiangsu-Singapore Joint Research Center for Organic/Bio-Electronics and Information Displays and Institute of Advanced Materials, Nanjing Tech University, Nanjing 211816, China*

(Received 10 March 2014; accepted 13 May 2014; published online 29 May 2014)

Two types of Au nanorods (NRs) possessing longitudinal/transverse axes of 55/11 (NR_{11}) and 90/18 nm (NR_{18}) are, respectively, incorporated into the hole extraction layer to improve optical-to-electrical conversion performances in polymer photovoltaic cells. Totally different improvement factors in short-circuit current and power conversion efficiency occur in the NR_{11}- and NR_{18}-doped cells. Optical simulations, electrical analysis, and morphology alteration accompanying with the incorporation of NRs were proceeded to investigate the reason, and analysis demonstrates that a slower damping of field around NRs_{18} (results in a field and absorption enhancement around the active layer) and one order higher scattering cross section in the NR_{18}-incorporated cell are key factors contributed to the improvement of cell performances.
 [http://dx.doi.org/10.1063/1.4880575]

Organic photovoltaic (OPV) cells are attracting many attentions due to their potential for low-cost, high-throughput processing. However, the excitonic bottleneck (exciton diffusion length of ~10 nm) in most organic polymers results in a tradeoff between light absorption and exciton harvesting efficiency in OPVs. Architectures used to overcome this problem have included bulk[1] and mixed[2] heterojunctions and the use of phosphorescent materials.[3] While the bulk heterojunction blended architecture partially alleviates the problem of exciton dissociation in optically thick films, the internal quantum efficiency (IQE) in bulk heterojunction cells often decreases rapidly with increasing film thickness. This drop in IQE is particularly significant for many new low band gap, red, and near-IR absorbing materials because they typically have lower absorption coefficients.[4] As an alternate approach, surface plasmons (SPs) have been exploited to improve the absorption efficiency. Ag and Au have dominated experimental researches in this area although other metals also support SPs. Up to now, there are many work exploring the influence of Au or Ag nanoparticles or nanostructures on OPV's performance by locating them into carrier extraction layer or active layer.[5–11] Unfortunately, the photocurrent enhancement from spherical Ag or Au nanoparticles is usually restricted due to their localized surface plasmon resonance (LSPR) around 430 nm and 530 nm, respectively. Here, it should be mentioned that rod-like Ag and Au nanostructures are attractive candidates since their longitudinal plasmon absorption can be tuned from visible, NIR and to the infrared region by simply manipulating the aspect ratio (AR),[12] providing a unique opportunity for utilizing the low energy range of the solar spectrum. In addition, Ag or Au nanorods (NRs) can be processed through wet chemical synthesis[13] with the well-dispersion in a variety of aqueous/organic solutions and their size, shape, density can also be easily controlled.[14] This approach of obtaining Ag or Au NRs present a less expensive choice compared with other methods, e.g., laser ablation,[15] electron beam lithography,[16] etc.

Although many researches on Au or Ag NR's synthesis methods and optical properties, theirs application in OPVs is rarely reported. Janković *et al.*[17] incorporated octadecyltrimethoxysilane (OTMS)-functionalized Au/SiO_2 core/shell NRs into active layers in 2013. They found that the greatest enhancement in power conversion efficiency (PCE) was observed in spectral regions where the OPV polymer absorbs poorly. In their work, they did not further explore quantitatively the field distribution around Au NRs induced by LSPR and not consider the influence of scattering on PCE at all. Hsiao *et al.*[18] first introduced series of Au nanospheres (NSs) with the LSPR peaks of 520, 530, and 540 nm and NRs with the longitudinal axis LSPR peaks of 660, 780, and 850 nm, covering from the visible to the NIR region, into OPVs to investigate the effects of the shape and size of Au NSs and NRs on optoelectrical performances in OPVs. By systematical analysis on film's extinction and photoluminescence (PL) spectra, they deduced that LSPR and light scattering, respectively, play an important and a minor role in the enhancement of OPV's performance, especially for Au NR780 (the LSPR peak of 780 nm). They also concluded that the integration of two kinds of Au NPs covering the whole absorption band-edge of the active layer is especially beneficial to the acquirement of a highest enhancement factor in OPVs, which is also powerfully proved recently by Lu *et al.* using Ag and

[a)]F. Cheng, Y. Mei, and B. Peng contributed equally to this work.
[b)]Authors to whom correspondence should be addressed. Electronic addresses: Qihua@ntu.edu.sg and iamdirector@njupt.edu.cn.

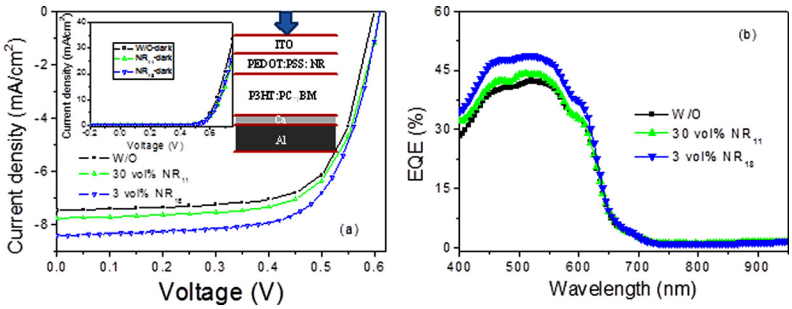

FIG. 1. (a) *J-V* and (b) EQE curves of P3HT:$PC_{71}BM$ devices without or with Au NRs. Inset is dark current characteristics and schematic structures for our OPV devices.

Au NSs with complementary absorption spectra.[19] In Hsiao's work,[18] differences of shapes, sizes, aspect ratios, absorption spectral ranges for those Au NSs or NRs bring too many variable factors, making rigorous analysis on a certain factor very difficult.

In order to further explore the influences of Au NRs on the optoelectrical conversion performances in OPVs and their major working mechanism, two kinds of Au NR, namely, NR_{11} and NR_{18} with the same AR but different sizes ($55 \pm 5/11 \pm 3$ and $90 \pm 10/18 \pm 3$ nm for NR_{11} and NR_{18}'s longitudinal/transverse axes) are used in this paper, where they generate the same LSPR wavelength in the NIR region (940 nm). Synthesis method of these NRs refers to Ref. 20. The NRs_{11} and NRs_{18} are, respectively, doped into the poly(3,4-ethylene dioxythiophene):poly(4-styrenesulfonate) (PEDOT:PSS) hole extraction layer to observe their influences on photovoltaic performances. Before use, the Au nanorods were centrifugated for about two times to remove reactants and stabilizing agents with the final concentration of $\sim 10^{17}$ particles/ml in aqueous solution. Each type of Au NR's concentration is further optimized to acquire the best OPV performance (with structure in the inset of Figure 1). For NR_{11}, the optimized volume ratio of rods to PEDOT:PSS is around 30%, resulting in a short-circuit current density (J_{sc}) and a PCE of 7.76 mA/cm^2 and 3.17%, compared to 7.48 mA/cm^2 and 3.07% in a standard cell without NRs, as the curves shown in Figure 1(a) and the result summarized in Table I. While for NRs_{18}, the optimal concentration is ~3%, and the corresponding J_{sc} and PCE exhibit enhancement factors of 12.2% and 12.7%, reaching 8.39 mA cm^{-2} and 3.46%, respectively. Both the corresponding external quantum efficiency (EQE) curves with an optimal NRs_{11} and NRs_{18} doping concentration (Figure 1(b)) exhibit some improvements over a wide wavelength range of 400–650 nm compared to that in the standard device, while for NRs_{18}, the magnitude of improvement is more significant, consistent with as-measured *J-V* characteristics. For both of the two kinds of NRs, the fill factor (FF) shows a slightly increase when using a low doping concentration and then gradually declines as the doping concentration becomes optimal in the OPVs.

TABLE I. Summary of the photovoltaic parameters with and without NRs.

NR's type	Rod concentration (v/v)	V_{oc} (V)	J_{sc} (mA/cm^2)	FF	PCE (%)
W/O	0	0.600	7.48	0.684	3.07
NR_{11}	30%	0.610	7.76	0.670	3.17
NR_{18}	3%	0.610	8.39	0.676	3.46

Photocurrent density (J_{ph}) versus effective voltage (V_{eff}) characteristic curves have been calculated to observe photogenerated excitons.[21] Here, J_{ph} is determined as $J_{ph} = J_L - J_D$, where J_L and J_D are the current density under illumination and in the dark, respectively. V_{eff} is determined as $V_{eff} = V_0 - V_a$, where V_0 is the voltage at which $J_{ph} = 0$ and V_a is the applied bias voltage. Figure 2 clearly shows that J_{ph} increases linearly at low V_{eff} values and saturates at a high V_{eff} (i.e., $V_{eff} > 0.6$ V). Assuming that all the photogenerated excitons are dissociated into free charge carriers and collected by electrodes afterward at a high V_{eff} region, saturation current density (J_{sat}) is then only limited by total amount of absorbed incident photons. G_{max} could be calculated from $J_{ph} = qG_{max}L$, where q is the electronic charge and L is the thickness of active layer (200 nm). The values of G_{max} for the control, NR_{11}- and NR_{18}-incorporated devices are 2.35×10^{27} m^{-3} s^{-1} ($J_{sat} = 75.2$ A/m^2), 2.45×10^{27} m^{-3} s^{-1} ($J_{sat} = 78.3$ A/m^2), and 2.56×10^{27} m^{-3} s^{-1} ($J_{sat} = 82$ A/m^2), respectively. Because the G_{max} value is only governed by the absorption of light,[7] the enhanced values suggest that the incorporation of the Au NR_{11} and NR_{18} increases the degree of light harvesting in the devices, which is further testified with the significant enhancement in the absorption spectra (Figure 3(a)) for the multilayer films of PEDOT:PSS:NR_{11} or NR_{18}/poly(3-hexylthiophene) (P3HT):[6, 6] phenyl C71-butyric acid methyl ester ($PC_{71}BM$) compared to the control PEDOT:PSS/P3HT:$PC_{71}BM$ film around 300–650 nm. From Figure 3(a), we also observe that the enhanced magnitude from NR_{18} is obviously higher than that from NR_{11}. To clearly explain this phenomenon, we simulate the absorption spectra of the NRs-doped PEDOT:PSS layer by using FDTD software. The calculation result shown in Figure 3(b) demonstrates that both Au NR_{11} and NR_{18} generate the same LSPR peaks with the longitudinal and

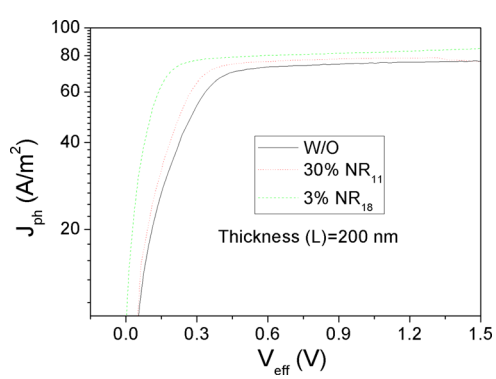

FIG. 2. Photocurrent density versus effective voltage for the OPVs with and without NRs.

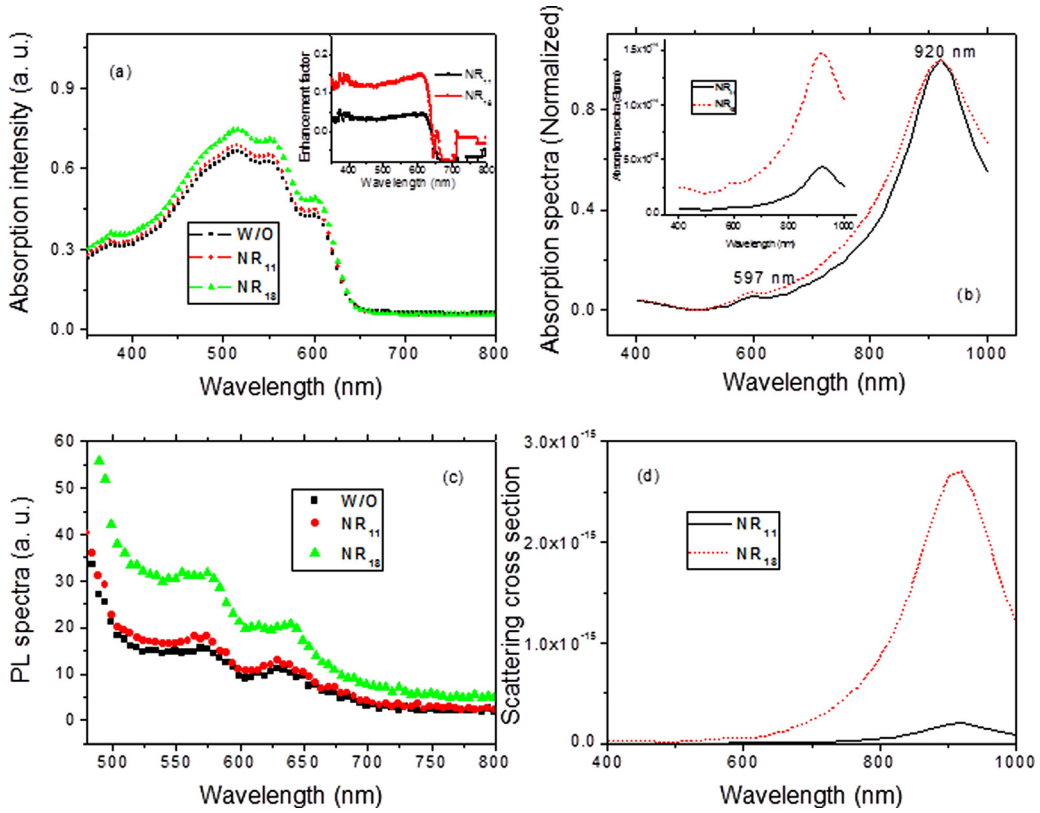

FIG. 3. (a) and (c) are the measured absorption and PL spectra of the PEDOT:PSS:NR_{11} or NR_{18}/P3HT:$PC_{71}BM$ films and the control film without NRs, (b) and (d) are calculated absorption spectra (normalized) and scattering cross sections of Au NR_{11} and NR_{18}. Inset of (a) and (b) are the enhancement factors of NRs' absorption and the calculated absolute absorption.

transverse axes peaks at 920 and 597 nm, respectively, but the absolute intensity from NR_{18} is one order higher than that from NR_{11}, as shown in the inset of Figure 3(b), indicating a much stronger absorption ability from NR_{18} and a larger local field intensity distribution around NR_{18}. From the simulation results of the field distribution around the NRs (Figure 4), one surprisingly observes that the largest electric field occurring at the surface of Au NR_{18} is almost equal to that at the surface of Au NR_{11} (excited with 597 nm, the resonance peak of transverse axis). Here, in order to obtain the above simulation results, it should be noted that we assumed that (1) the ideal distribution of NRs is in the layer center of the 50-nm thick PEDOT:PSS, (2) most of Au NRs lie but not stand in the PEDOT:PSS film, (3) x axis is along the longitudinal axis of Au NRs and z axis (the incident direction of sun light is along with the backwards of z axis) is perpendicular to the PEDOT:PSS film, and (4) the periodic distribution of Au NRs is 200 nm × 200 nm. However, from careful comparison of the local field around NRs in Figure 4(c), we find that although the field quickly declines down to 1 for both NR_{11} and NR_{18} when far away from the surface of Au NR, the field intensity around NR_{11} decreases more quickly than that around NR_{18}, with no more gain when the distance from the center of NR_{11} is larger than 21 nm, indicating the active layer cannot absorb the additive energy generated by LSPR for a 50-nm thick PEDOT:PSS film if the NRs are mainly distributed in the center of the PEDOT:PSS film. In contrast, the field around NR_{18} showing a slower damping can extend to 38 nm away from the center of the NR structure and maintain about 1.2 times of the

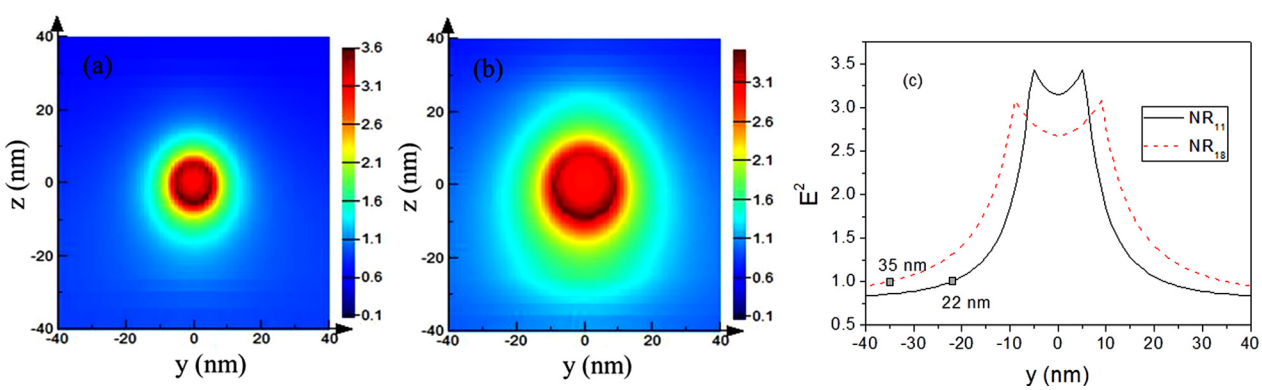

FIG. 4. The distribution of the electric field intensity around Au (a) NR_{11} and (b) NR_{18} along yz plane, and (c) is the comparison of the NR_{11} and NR_{18} electric field intensities along y axis under z = 0.

incident field intensity ($|E|^2$) even at the P3HT/PEDOT:PSS interface, thus resulting in the PL enhancement of the P3HT active layer considering of the overall increase in PL intensity proportional to $|1.2E|^2$ due to LSPR.[22] This can be further proved with the measurement of the PL spectra for the PEDOT:PSS:NR_{11} or NR_{18}/P3HT:$PC_{71}BM$ films (Figure 3(c)). A slight enhancement for the PEDOT:PSS:NR_{11}/P3HT:$PC_{71}BM$ film compared to the non-doped one in Figure 3(c) indicates the Au NRs are randomly distributed and not totally lied in the center of the PEDOT:PSS layer. From above measurement of the absorption and PL spectra and the simulation work on the local field around Au NRs, we can clearly explain the obvious J_{sc} and PCE improvement in the NR_{18}-doped OPVs.

Besides the magnified electric field generated by LSPR, the influence of scattering from Au NRs should be taken for granted to be considered. Our common sense tells us that a large-size NR, e.g., NR_{18}, will bring larger scattering intensity than the small one and result in lengthened light transport path, which further increases light absorption in OPV cells. The above idea has been identified by the simulated scattering cross section, as shown in Figure 3(d), from which one observes that the scattering cross section from NR_{18} is one order higher than that from NR_{11}. As a conclusion, the OPVs doping NR_{18} show a higher photon-to-electrical conversion performance due to both LSPR-induced field enhancement and the relatively large scattering cross section.

In addition to the absorbance and scattering enhancement in the NRs_{18}-doped OPVs, other possible factors, such as the alteration of the hole extraction and transport ability induced by Au NRs_{18} and the morphology changes of the PEDOT:PSS film by incorporating Au NRs, have been further investigated to observe their influences on solar cells. Hole- and electron-dominated single-carrier devices with the structures of ITO/PEDOT:PSS (~50 nm, with 3% or without Au NR_{18})/Ag and ITO/LiF (1 nm)/PEDOT:PSS (~50 nm, with 3% or without Au NR_{18})/Ca/Ag have been designed in order to observe the influence of NRs. The *J-V* curves (not shown here) indicate that the incorporation of Au NRs_{18} brings no obvious alteration in injection and transport of the current, indicating a negligible influence of the shallow impurity energy level induced by Au on hole extraction and transport.[23]

It has been suggested that a rough P3HT:PCBM surface creates defect sites that assist exciton dissociation.[24] Besides, increasing anode surface roughness will increase the interface area between the anode and the active layer, providing shorter routes for holes to travel to the anode and enhancing hole collection at the anode.[25] The increased interfacial area between PEDOT:PSS and P3HT:PCBM allows the collection of a larger number of holes in the P3HT:PCBM layer, thus increasing J_{sc}. Thus, the morphology changes of the PEDOT:PSS layer with 3% or with the absence of Au NRs_{18} are measured by applying atomic force microscopy on the PEDOT:PSS or PEDOT:PSS:Au NRs_{18} film. With introducing the Au NR_{18}, we observe a slight change in surface morphology of the rod-doped PEDOT:PSS film with an increase in surface roughness (R_a) from 1.53 to 1.63 nm. This result indicates that the doping of NRs_{18} is beneficial to exciton dissociation and the collection of a larger number of holes to some extent, resulting in the increase in J_{sc}, but we simultaneously infer that the roughness-induced increase in J_{sc} will not be significant due to a small alteration of R_a.

In conclusion, two types of Au NRs possessing longitudinal/transverse axes of 55/11 (NR_{11}) and 90/18 nm (NR_{18}) are, respectively, incorporated into PEDOT:PSS to improve the OPV performances. Totally different improvement factors in J_{sc} and PCE are obtained in the NR_{11}- and NR_{18}-doped cells, indicating the introduction of NR_{11} and NR_{18} into the PEDOT:PSS layer brings different influences on distribution and transport of light. To explore the origin of the improved performance, several characterizations including optical simulation, electrical transport performance, and film morphology have been investigated. Simulation results demonstrate that NR_{18} generates a similar electric field intensity with NR_{11} at the rods/PEDOT:PSS interface but a slower damping of field around NRs_{18}, which keeps an enhanced field when reaching the active layer in NR_{18}-doped cells. In addition, the scattering cross section from NR_{18} is one order higher than that from NR_{11}. The incorporation of NRs_{18} results in a slight increase in surface roughness of the PEDOT:PSS film, which is beneficial to exciton dissociation and the collection of a larger number of holes to some extent. Both the enhanced field intensity around rods and large scattering from NRs_{18}, together with a slight increase in surface roughness of the film contribute to the improved cell performances.

The authors acknowledge financial support from the Ministry of Science and Technology (Grant No. 2012CB933301), NSFC(Grant Nos. 61274065, 60907047, 51173081, 61136003, and BZ2010043). Q.H.X. gratefully thanks the strong support from Singapore National Research Foundation through a Competitive Research Program (NRF-CRP-6-2010-2), Singapore Ministry of Education via two Tier2 grants (MOE2011-T2-2-051 and MOE2011-T2-2-085).

[1]J. J. M. Halls, C. A. Walsh, N. C. Greenham, E. A. Marseglia, R. H. Friend, S. C. Moratti, and A. B. Holmes, Nature **376**, 498 (1995).
[2]J. Xue, B. P. Rand, S. Uchida, and S. R. Forrest, Adv. Mater. **17**, 66 (2005).
[3]G. Yu, J. Gao, J. C. Hummelen, F. Wudl, and A. J. Heeger, Science **270**, 1789 (1995).
[4]O. Inganas, F. Zhang, and M. R. Andersson, Acc. Chem. Res. **42**, 1731 (2009).
[5]O. Stenzel, A. Stendal, K. Voigtsberger, and C. von Borczyskowski, Sol. Energy Mater. Sol. Cells **37**, 337 (1995).
[6]B. P. Rand, P. Peumans, and S. R. Forrest, J. Appl. Phys. **96**, 7519 (2004).
[7]F. C. Chen, J. L. Wu, C. L. Lee, Y. Hong, C. H. Kuo, and M. H. Huang, Appl. Phys. Lett. **95**, 013305 (2009).
[8]A. P. Kulkarni, K. M. Noone, K. Munechika, S. R. Guyer, and D. S. Ginger, Nano Lett. **10**, 1501 (2010).
[9]D. H. Wang, D. Y. Kim, K. W. Choi, J. H. Seo, S. H. Im, J. H. Park, O. O. Park, and A. J. Heeger, Angew. Chem. Int. Ed. **50**, 5519 (2011).
[10]D. D. S. Fung, L. Qiao, W. C. H. Choy, C. Wang, W. E. I. Sha, F. Xie, and S. He, J. Mater. Chem. **21**, 16349 (2011).
[11]X. Li, W. C. H. Choy, L. Huo, F. Xie, W. E. I. Sha, B. Ding, X. Guo, Y. Li, J. Hou, J. You, and Y. Yang, Adv. Mater. **24**, 3046 (2012).
[12]J. Pérez-Juste, I. Pastoriza-Santos, L. M. Liz-Marzán, and P. Mulvaney, Coord. Chem. Rev. **249**, 1870 (2005).
[13]N. R. Jana, L. Gearheart, and C. J. Murphy, Chem. Commun. **2001**, 617.
[14]B. Nikoobakht and M. A. El-Sayed, J. Phys. Chem. A **107**, 3372 (2003).

[15]J. Bosbach, D. Martin, F. Stietz, T. Wenzel, and F. Trager, Appl. Phys. Lett. **74**, 2605 (1999).
[16]N. Felidj, J. Aubard, G. Levi, J. R. Krenn, M. Salerno, G. Schider, B. Lamprecht, A. Leitner, and F. R. Aussenegg, Phys. Rev. B **65**, 075419 (2002).
[17]V. Janković, Y. Yang, J. B. You, L. T. Dou, Y. S. Liu, P. Cheung, J. P. Chang, and Y. Yang, ACS Nano **7**, 3815 (2013).
[18]Y.-S. Hsiao, S. Charan, F.-Y. Wu, F.-C. Chien, C.-W. Chu, P. Chen, and F.-C. Chen, J. Phys. Chem. C. **116**, 20731 (2012).
[19]L. Y. Lu, Z. Q. Luo, T. Xu, and L. P. Yu, Nano Lett. **13**, 59 (2013).
[20]B. Peng, G. Li, D. Li, S. Dodson, Q. Zhang, J. Zhang, Y. H. Lee, H. V. Demir, X. Y. Ling, and Q. H. Xiong, ACS Nano **7**, 5993 (2013).
[21]V. D. Mihailetchi, J. Wildeman, and P. W. M. Blom, Phys. Rev. Lett. **94**, 126602 (2005).
[22]S. Kühn, U. Håkanson, L. Rogobete, and V. Sandoghdar, Phys. Rev. Lett. **97**, 017402 (2006).
[23]K. Kim and D. L. Carroll, Appl. Phys. Lett. **87**, 203113 (2005).
[24]G. Li, V. Shrotriya, Y. Yao, and Y. Yang, J. Appl. Phys. **98**, 043704 (2005).
[25]M.-H. Hsu, P. Yu, J.-H. Huang, C.-H. Chang, C.-W. Wu, Y.-C. Cheng, and C.-W. Chu, Appl. Phys. Lett. **98**, 073308 (2011).